Hyperspectral fluorescence image analysis for use in medical diagnostics

Seong G. Kong[*a], Zheng Du[a], Matthew Martin[b], Tuan Vo-Dinh[b]
[a]Dept. of Electrical and Computer Engineering, The Univ. of Tennessee, Knoxville, TN USA 37996;
[b]Life Science Division, Oak Ridge National Laboratory, Oak Ridge, TN USA 37831-6101

ABSTRACT

This paper presents hyperspectral fluorescence imaging and a support vector machine for detecting skin tumors. Skin cancers may not be visually obvious since the visual signature appears as shape distortion rather than discoloration. As a definitive test for cancer diagnosis, skin biopsy requires both trained professionals and significant waiting time. Hyperspectral fluorescence imaging offers an instant, non-invasive diagnostic procedure based on the analysis of the spectral signatures of skin tissue. A hyperspectral image contains spatial information measured at a sequence of individual wavelength across a sufficiently broad spectral band at high-resolution spectrum. Fluorescence is a phenomenon where light is absorbed at a given wavelength and then is normally followed by the emission of light at a longer wavelength. Fluorescence generated by the skin tissue is collected and analyzed to determine whether cancer exists. Oak Ridge National Laboratory developed an endoscopic hyperspectral imaging system capable of fluorescence imaging for skin cancer detection. This hyperspectral imaging system captures hyperspectral images of 21 spectral bands of wavelength ranging from 440 nm to 640 nm. Each band image is spatially co-registered to eliminate the spectral offset caused during the image capture procedure. Image smoothing by means of a local spatial filter with Gaussian kernel increases the classification accuracy and reduces false positives. Experiments show that the SVM classification with spatial filtering achieves high skin tumor detection accuracies.

Keywords: Hyperspectral imaging, Fluorescence image, Tumor detection, Medical diagnostics

1. INTRODUCTION

Skin cancer is one of the most common cancers in the United States with over 59,350 cases diagnosed in 2004[1]. Early diagnosis and thorough treatment are the keys to gaining a favorable prognosis. Cancer causes the cells grow out of control to form tumors. Current skin cancer diagnostic methods often rely on skin biopsy that involves the removal of tissue samples from the body for examination. Despite being a definitive test of skin cancer, the biopsy is an invasive and subjective diagnostic technique that requires both trained professionals and significant waiting time. A significant number of false positives may undergo biopsy or many malignant lesions can be overlooked. Developing non-invasive and objective techniques will be highly desirable in medical diagnostics.

Optical imaging has been used extensively in the desire to develop a non-invasive diagnostic procedure[2]. Hyperspectral imaging sensor collects the electromagnetic spectrum at dozens or hundreds of wavelength ranges in the spectra and produce high-dimensional spectral signature data. Hyperspectral image data contains spatial information measured at a sequence of individual wavelength across a sufficiently broad spectral band. High-dimensional spectral signatures provide a detailed discrimination of the scene and therefore increase classification accuracies. The spectral signatures are useful for identifying various tissue compositions due to their unique spectral characteristics at different wavelengths[3,4]. In clinical diagnostics, hyperspectral imaging provides an effective method for early detection as well as monitoring of the effectiveness of therapy for retinal disease[5]. Hyperspectral imaging has been of critical importance to help the food processing industry inspect wholesomeness in meat products[6].

[*] skong@utk.edu; phone 1 865 974-3861; fax 1 865 974-5483

This paper presents endoscopic imaging of hyperspectral fluorescence images and a spectral signature analysis method for use in skin tumor diagnostics. Hyperspectral fluorescence imaging offers an instant, non-invasive inspection method for detecting biomedical abnormalities such as skin tumors[7]. Fluorescence is a phenomenon where light is absorbed at a given wavelength and then is normally followed by the emission of light at a longer wavelength. Fluorescence techniques are generally regarded as sensitive optical tools and have proven to be useful in a number of scientific areas[8]. There are a number of compounds that emit fluorescence in the visible range when excited with ultraviolet radiation. The altered biochemical and morphological state of the neoplastic tissue is reflected in the spectral characteristics of the measured fluorescence. Figure 1 shows the proposed procedure of hyperspectral image analysis for skin tumor detection. Hyperspectral images captured by the imaging system are not perfectly aligned since the acousto-optic tunable filter (AOTF) diffract light on each different wavelength and causes the translation between every spectral image. Image registration process finds a geometric transformation to spatially align the images. Mutual information is used to find the offsets between the spectral band images. A Gaussian filter finds local averaging of spectral signatures to reduce the noise effect. A support vector machine (SVM) pattern classifier is developed to detect skin tumor from the hyperspectral fluorescence image. Classification results show that the spectral signature analysis method efficiently detects skin tumors from hyperspectral fluorescence images.

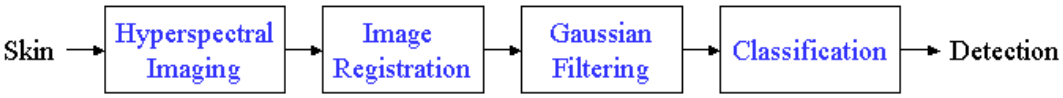

Figure 1: Procedure of hyperspectral image analysis for mouse tumor detection

2. HYPERSPECTRAL FLUORESCENCE IMAGE ACQUISITION

2.1 Imaging system

Oak Ridge National Laboratory has developed a hyperspectral imaging system capable of fluorescence imaging for skin tumor detection. Figure 2 shows hardware components of the imaging system: an imaging fiber probe system for signal collection, an endoscope, an acousto-optic tunable filter for wavelength selection, a laser excitation source, an endoscopic illuminator, a CCD color camera for reflection detection, and an intensified charge-coupled device (ICCD) for fluorescence detection. Reflection images were acquired using an endoscopic illuminator (Olympus Model CLV-10) equipped with a 300-watt CW Xe arc lamp source. The reflection source was coupled to a gastrointestinal endoscope (Olympus Type T120) equipped with an imaging bundle. Fluorescence spectra and images were acquired using a LSI pulsed Nitrogen laser (Model VSL-337) with a maximum repetition rate of 20 Hertz. For fluorescence imaging, the N_2-pumped laser was coupled to a bifurcated fiber probe (R400-7-VIS/NIR) that was also used to sample point measurements using a miniature fiber optic spectrometer (Ocean Optics USB2000-FLG).

Data produced by hyperspectral imaging systems are essentially a three dimensional cube of data $I(x, y, \lambda_i)$, $x = 0, 1, \ldots, M-1$, $y = 0, 1, \ldots, N-1$. The x and y denote the spatial coordinates a pixel location in the image and λ_i $(i=1,2,\ldots,L)$ denotes a spectral band (wavelength range). The value stored at $I(x, y, \lambda_i)$ is the response from the pixel (x, y) at a wavelength corresponding to the wavelength λ_i.

2.2 Hyperspectral fluorescence image acquisition

Both fluorescence and scattered light were collected through the endoscope into the AOTF device via collimating lenses. The AOTF has a dynamic range of 400-650 nm with a 10×10 mm aperture and a spectral resolution of 1-2 nm. The fluorescent light emitted by the tissues is diffracted by the AOTF (Brimrose TEAF10-0.4-0.65-S) at a 60-degree angle from the undiffracted (zero-order) beam thus separating the reflected image from the fluorescent image. A mirror placed in front of the AOTF projected the acquired images onto the ICCD (Model IMAX-512-T-18 Gen. II) camera for fluorescence imaging and onto the CCD camera (Sony Model CCD-Iris) for reflection imaging. Individual wavelengths can be diffracted by the AOTF and thus sent to the ICCD. A Brimrose AOTF controller (Model VFI-160-80-DDS-A-

C2) controls the AOTF. The controller sends an RF signal to the AOTF based on the input provided by the researcher using the Brimrose software. Wavelength selection takes place in microseconds enabling ultra-fast modulation of wavelength output to the ICCD. Wavelength specific images were taken between 440-650 nm every ten nanometers. In addition to the imaging capability, spectral information from each site was obtained using the Ocean Optics spectrometer coupled to a laptop computer.

A timing generator incorporated into the ICCD camera controller (ST-133) allowed the ICCD to operate in the pulsed mode with a wide range of programmable functions. Fluorescence images were acquired by gating the intensified ICCD camera. A 500 ns delay between the laser trigger and the detector activation was programmed to synchronize the laser and the detector. The intensifier was gated for 500 ns during which a 5 ns laser pulse was delivered to the tissues. An image was captured twenty times per second, integrated by internal software, and output to a screen once per second. This allows for real time fluorescence detection. Fluorescence images and spectra were acquired and processed with WinView (Roper Scientific) and OOIBase32 (Ocean Optics) software respectively. Reflection images were captured and processed with SimplePCI image analysis software (Compix).

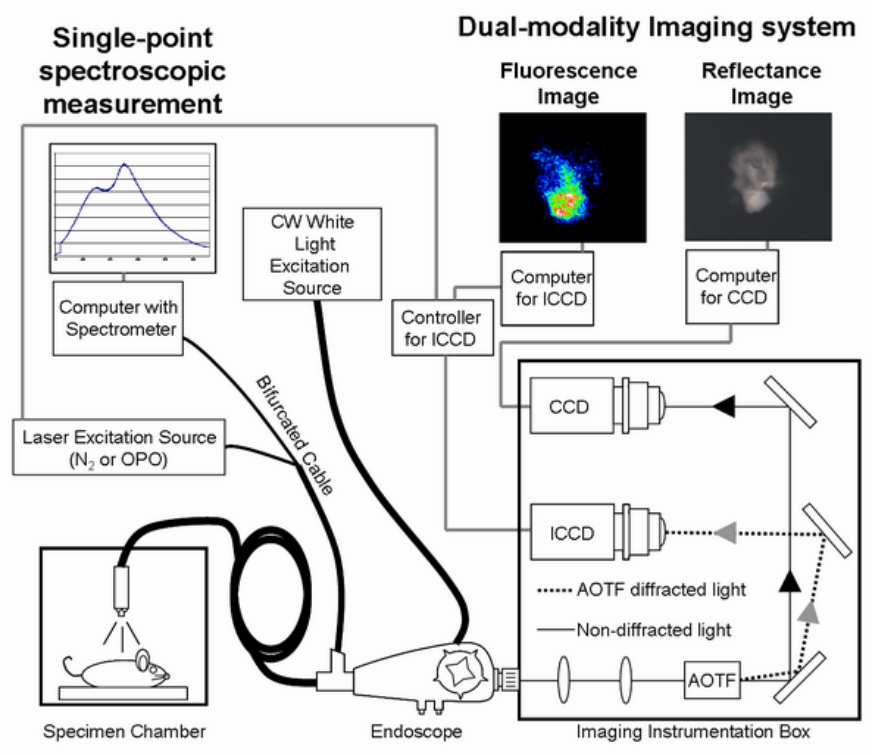

Figure 2: Hardware components of the hyperspectral imaging system

3. SPECTRAL SIGNATURE EXTRACTION

3.1 Registration of hyperspectral band images

In order to obtain accurate spectral information of each pixel, all spectral band images must be aligned. Image registration is the process to find a geometric transformation of multiple images of the same scene taken at different wavelengths. The correspondence between the images is maximized when an image pair is correctly aligned. Mutual information[9] (MI) is used as a metric for searching the offset of the band images along the horizontal axis. The MI measures the similarity of the two images in terms of the Kullback-Leibler distance. An image pair with maximum MI shows the best match between a reference image and an input image. The offsets along the horizontal axis are found for

all spectral band images using the MI. Misregistration of the images will result in the decrease of the MI. Figure 3(a) shows the offsets obtained from a hyperspectral fluorescence image. The band image at the wavelength of 490 nm is used as a reference image due to its strongest fluorescence intensity. The input images with positive offset values should be shifted to the right for correct registration. Figure 3(b) demonstrates a registration example of two band images. The input band image (540 nm) was shifted left by the amount of offset (14 pixels) with respect to the reference image (490 nm).

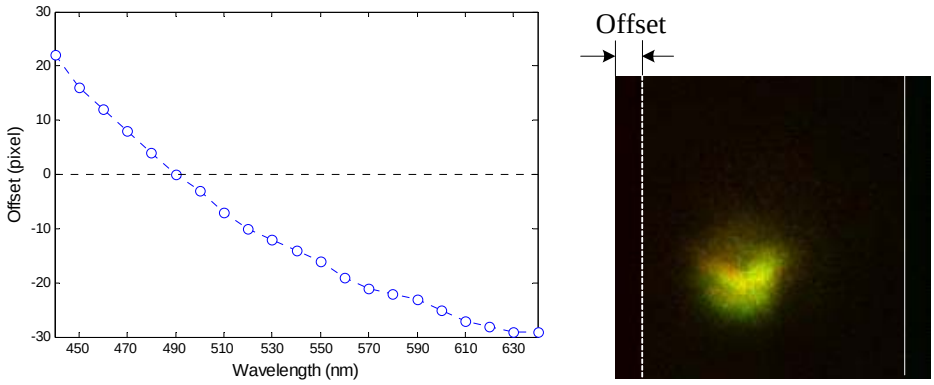

(a) The offsets along the horizontal axis (b) Registration of the band images

Figure 3: Spatial registration of hyperspectral band images. (a) Offsets along the *x*-axis caused by the AOTF at each wavelet, (b) Registration example of spectral band images with the wavelengths 490 nm and 540 nm

3.2 Spectral signatures of mouse skin

Tissues emit different amount of fluorescence intensity at different wavelengths of the electromagnetic spectrum. Spectral characteristics of the measured fluorescence in different wavelength regions yield a distinguishable spectral signature, making different skin types distinguishable. Figure 4 shows the relative fluorescence intensity of normal tissue and tumor as a function of spectral bands (wavelength). Normal tissues have higher fluorescence intensity on average than the tumor regions. Normal tissues have a peak fluorescence response near the wavelength 490 nm. Tumors also show strong responses between the bands 480 nm to 500 nm. The intensity difference between the two classes is large in the spectral range of 470-560 nm. Spectral characteristics of the pixels from the two categories can be used as the features for tumor detection.

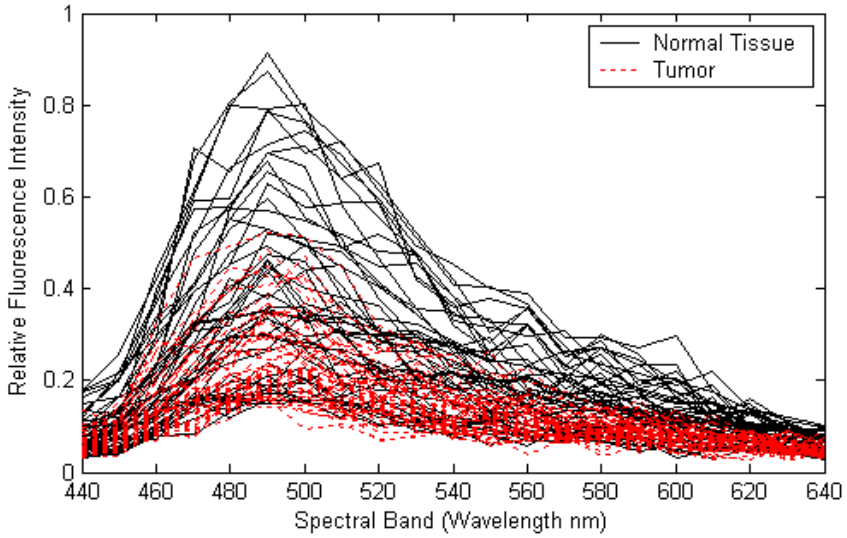

Figure 4: Spectral signature of the normal tissue and tumor

4. SUPPORT VECTOR MACHINES FOR TUMOR DIAGNOSIS

4.1 Spectral signature classification with support vector machines

Support vector machine is a learning system based on the statistical learning theory[10,11] SVM aims at producing a pattern classifier with maximum margin of class separation to maximize the generalization ability. The separating margin is defined as the distance between the classification boundary and the nearest data point of each class. Large separation margin minimizes structural risk of misclassification and improves classification accuracies for unseen data. Consider the problem of separating a set of training vectors that belong to two separate classes. Let $\boldsymbol{x}_j$ be a column vector and $y_j = \{+1, -1\}$ denote binary class label for $\boldsymbol{x}_j$. The data is said to be *linearly separable* by the separating hyperplane $\boldsymbol{w}^t \boldsymbol{x} + b = 0$ if there exist a vector $\boldsymbol{w}$ and a scalar b such that

$$\boldsymbol{w}^t \boldsymbol{x}_j + b \geq 1 \quad \text{if} \quad y_j = +1 \tag{1}$$

$$\boldsymbol{w}^t \boldsymbol{x}_j + b < -1 \quad \text{if} \quad y_j = -1 \tag{2}$$

These can be combined into one set of inequalities:

$$\left[y_j \left(\boldsymbol{w}^t \boldsymbol{x}_j + b \right) - 1 \right] \geq 0 \tag{3}$$

Then the separating margin between the two classes becomes to $2/\|\boldsymbol{w}\|$. To maximize the margin, the norm $\|\boldsymbol{w}\|$ needs to be minimized with the limitation given in (3). A Lagrange function is used to represent the constrained optimization problem:

$$L(\boldsymbol{w}, b, \alpha) = \frac{1}{2}\|\boldsymbol{w}\|^2 - \sum_{j=1}^{l} \alpha_j \left[y_j \left(\boldsymbol{w}^t \boldsymbol{x}_j + b \right) - 1 \right] \tag{4}$$

where α_j is called a Lagrange multiplier. After solving the criterion function, the discriminant function to classify a new pattern $\boldsymbol{x}$ can be represented by a small subset of support vectors $\boldsymbol{x}_j$:

$$f(\boldsymbol{x}) = \operatorname{sgn}\left(\sum_j y_j \boldsymbol{\alpha}_j \left\langle \boldsymbol{x} \cdot \boldsymbol{x}_j \right\rangle + b \right) \tag{5}$$

Equation (5) indicates that the decision function depends on the inner product between the patterns. For not linearly separable cases, a nonlinear transform function $\Phi(\cdot)$ is used to map the input vectors to higher dimensional feature space, which is more likely linearly separable. Nonlinear decision boundaries in the input space will be mapped to linear decision boundaries in the feature space. The classification function can be represented by the kernel function $K(\boldsymbol{x}_i, \boldsymbol{x}_j) = \Phi(\boldsymbol{x}_i) \cdot \Phi(\boldsymbol{x}_j)$ in the transformed feature space. The nonlinear transform function $\Phi(\boldsymbol{x}_i)$ needs not be specified. Using the kernel function, the discriminant function for a nonlinearly separable problem can be similarly written as

$$f(\boldsymbol{x}) = \operatorname{sgn}\left(\sum_j y_j \boldsymbol{\alpha}_j K(\boldsymbol{x}, \boldsymbol{x}_j) + b \right) \tag{6}$$

The optimal decision boundary for detecting skin tumors is obtained using the kernel SVM. In this paper, a Gaussian radial-basis function (RBF) kernel is used:

$$K(\boldsymbol{x}, \boldsymbol{x}_j) = \exp\left(-\left\| \boldsymbol{x} - \boldsymbol{x}_j \right\|^2 / 2\sigma^2 \right) \tag{7}$$

where σ is the parameter that controls the width of the Gaussian kernel function. A practical problem for training an SVM is the choice of kernel parameters. An optimal parameter value is found for a specific dataset to reduce the risk of overfitting and therefore poor generalization. An optimal parameter is found by doing cross-validation in the training process. Classification was repeated using 25% training and 75% validation data randomly chosen. The parameter σ =

0.1 was chosen as the optimal value that correspond to the lowest validation error. A SVM implementation[12] is used to perform the SVM training and classification.

4.2 Spatial filtering for the combination of spatial and spectral information

In hyperspectral image processing, spatial information provides useful information to increase the accuracy for detecting the object of interest. Tumors are likely present in a form of ellipsoidal shapes, not isolated points, with homogeneous texture properties. A spatial filtering technique is proposed to combine the spectral and spatial information for increasing the classification accuracy. The filtering process removes the noise in the hyperspectral image and enhances the texture information. Fluorescence intensity at each pixel is replaced by the weighted average of the neighborhood. Before classification

Filtering of a hyperspectral image with a filter mask $w(s,t)$ of size $m \times n$ is given by the expression:

$$g(x, y, \lambda_i) = \sum_{s=-a}^{a} \sum_{t=-b}^{b} w(s,t) I(x+s, y+t, \lambda_i) \tag{8}$$

where $w(s,t)$ denotes filter mask coefficients, $a=(m-1)/2$ and $b=(n-1)/2$. To generate a complete filtered image this equation must be applied for $x = 0, 1, \ldots, M-1$ and $y = 0, 1, \ldots, N-1$. A Gaussian filter mask is used to yield a weighted average of the pixels in a small neighborhood. Figure 5 shows an integer-valued 5×5 Gaussian filter kernel that approximates a Gaussian distribution with unit variance.

$$w(s,t) = \frac{1}{273} \begin{bmatrix} 1 & 4 & 7 & 4 & 1 \\ 4 & 16 & 26 & 16 & 4 \\ 7 & 26 & 41 & 26 & 7 \\ 4 & 16 & 26 & 16 & 4 \\ 1 & 4 & 7 & 4 & 1 \end{bmatrix}$$

Figure 5: A 5×5 Gaussian filter mask

5. EXPERIMENT RESULTS

5.1 Test data description

Hyperspectral fluorescence image samples are taken from the mouse skin using the Oak Ridge National Laboratory imaging system. The hyperspectral data consists of the size 165×172 pixels with 21 spectral bands ranging from the wavelength λ_1 (440 nm) to λ_{21} (640 nm) with 10 nm spectral resolutions. A small area of interest is well illuminated and the fluorescence intensity of the background is uniformly low. Figure 6(a) is a reflectance image and Figure 6(b) shows a fluorescence image at the wavelength 490 nm from a mouse skin sample with a tumor spot. The region of interest (ROI) is segmented out of the background as in Figure 6(c). The U-shaped, bright area in the fluorescence image is normal tissue, and the gray part above the normal skin corresponds to the tumor.

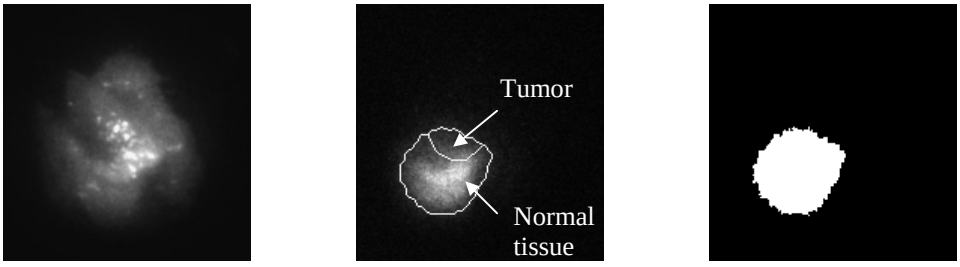

(a) Reflection image (b) Fluorescence image (490 nm) (c) Region of interest

Figure 6: Sample fluorescence image of mouse skin tumor

Decision boundaries of the kernel SVM with Gaussian radial-basis functions are developed using the mouse skin samples selected randomly from the two classes. The SVM parameters are trained from 100 samples chosen randomly from each of the normal and tumor class. For testing, 2036 (normal) and 517 (tumor) samples are used.

5.2 Performance comparisons

The performance of the SVM classifier and the spatial filtering method are evaluated. Pixels of a mouse sample are classified by the use of SVM classifiers with and without spatial filtering. SVM classifier with a 5×5 Gaussian spatial filtering is tested. The overall accuracy[13] is calculated as the total number of correctly classified pixels divided by the total number of pixels. The classification accuracies are summarized in Table 1. The Gaussian smoothing successfully classifies 514 tumor pixels with the classification accuracy of 99% for tumor. Normal tissues are classified as 83%. Most misclassified pixels of the normal tissue are on the edge of the ROI mainly due to poor illumination on the edge. The illumination leads the fluorescence intensity of the normal tissue in this area similar to the fluorescence intensity of the tumor. Experiment results clearly show that the spatial filtering enhances the best performance, which result in 86% overall accuracy, followed by using the original data (83%). In terms of the tumor accuracy, the neural network algorithm still exhibited the best accuracy (99%). The classification accuracy degrades from 83% to 56% after using feature extraction. This suggests that the SVM classifier can get better performance on high dimensional data. All these results demonstrate the efficiency of the information integration algorithm for the classification of hyperspectral image.

Table 1: Comparisons of classification accuracies

Method	Normal pixels	Tumor pixels	Classification Accuracies (%)		
			Normal	Tumor	Overall
Ground truth	2036	517	-	-	-
SVM without filtering	1651	466	81	90	83
SVM with Gaussian smoothing	1687	514	83	99	86

Figure 7 shows the classification results of the SVM-based classification. White pixels indicate the tumor region detected by the classifier while gray pixels denote normal tissues. In Figure 7(a), a large number of false positives and false negatives are present, especially along the edge of the ROI due to poor illumination. The SVM classifier with Gaussian filtering significantly improved the classification accuracies by reducing false positive and false negative pixels.

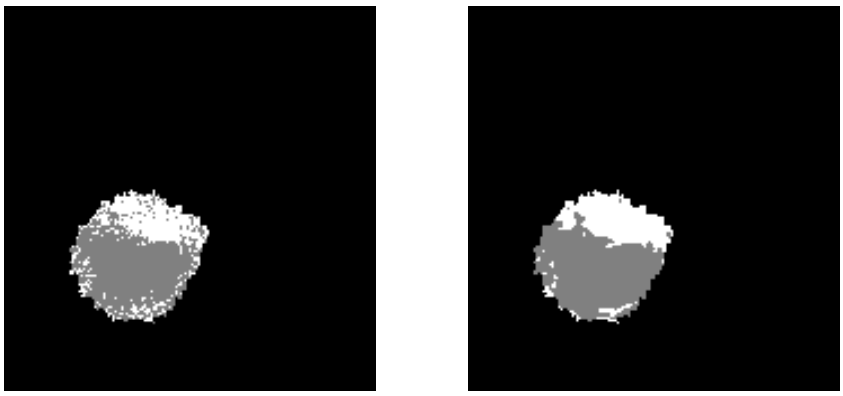

(a) SVM classification (b) SVM with Gaussian smoothing

Figure 7: Classification results

6. CONCLUSION

This paper presents hyperspectral fluorescence imaging and an efficient analysis method for use in medical diagnostics especially in skin tumor detection. The proposed diagnostic method combines the hyperspectral fluorescence imaging and support vector machine pattern classifier to obtain high classification accuracy of skin tumors. The hyperspectral imaging system developed by the Oak Ridge National Laboratory is capable of capturing hyperspectral fluorescence imaging for skin cancer detection. Skin tumor is not as visually obvious as other pathological diseases since its signature appears as shape distortion rather than discoloration. This fact makes it difficult to detect skin tumor patterns from the images based on reflections. Fluorescence data captured by the hyperspectral imaging system contains a higher level of spectral details and thus provide a greater possibility of detecting tumors. In order to eliminate the spatial offset in the spectral band images, mutual information is utilized as a measure to find the offsets along the horizontal axis. The offsets found are used to bring the band images into spatial correspondence. A support vector machine with Gaussian radial-basis function kernel provides a decision boundary with maximum margin of class separability. A Gaussian filtering integrates the spatial information by replacing the fluorescence intensity of each pixel by the weighted average values within a small neighborhood. Experiments show that this method achieved 99% classification accuracy for tumor tissue and 86% overall accuracy.

REFERENCES

1. American Cancer Society, *Cancer Facts and Figures*, p.4, Atlanta, GA, 2004.
2. J. Zhang, C. Chang, S. Miller, and K. Kang, "Optical biopsy of skin tumors," *Proc. 21st Annual Conference on Engineering in Medicine and Biology*, Vol. 2, pp.13-16, Oct. 1999.
3. G. Shaw and D. Manolakis, "Signal processing for hyperspectral image exploitation," *IEEE Signal Processing Magazine*, Vol. 19, No. 1, pp.12-16, Jan. 2002.
4. D. Landgrebe, "Hyperspectral image data analysis," *IEEE Signal Processing Magazine*, Vol.19, No. 1, pp. 17-28, Jan. 2002.
5. D. Cohen, M. Arnoldussen, G, Bearman, and W. Grundfest, "The Use of Spectral Imaging for the Diagnosis of Retinal Disease," *Proc. 12th Annual Meeting of Lasers and Electro-Optics Society*, Vol. 1, pp.220-221, Nov. 1999.
6. K. Chao, P. Mehl, and Y. Chen, "Use of hyper- and multi-spectral imaging for detection of chicken skin tumors," *Applied Engineering in Agriculture*, Vol. 18, No. 1 pp.113-119, 2002.
7. S. G. Kong, Y. R. Chen, I. Kim, and M. S. Kim, "Analysis of Hyperspectral Fluorescence Images for Poultry Skin Tumor Inspection," *Applied Optics*, Vol. 43, No. 4, pp.824-833, 2004.
8. B. Albers, J. DiBenedetto, S. Lutz, and C. Purdy, "More Efficient Environmental Monitoring with Laser-induced fluorescence Imaging," *Biophotonics International Magazine*, Vol. 2, No. 6, pp.42-54, Nov. 1995.
9. J. Pluim, J. Maintz, and M. Viergever, "Mutual-information-based registration of medical images: a survey," *IEEE Transactions on Medical Imaging*, Vol. 22, No. 8, pp.986-1004, 2003.
10. V. Vapnik, *The Nature of Statistical Learning Theory*, New York: Springer-Verlag, 1995.
11. V. Vapnik, *Statistical Learning Theory*, New York: John Wiley & Sons, 1998.
12. S. Gunn, "Support Vector Machines for Classification and Regression," *Technical Report MP-TR-98-05*, *Department of Electronics and Computer Science, University of Southampton*, 1998.
13. R. Congalton, "A review of assessing the accuracy of classifications of remotely sensed data," *Remote Sensing of Environment*, Vol. 37, pp.35-46, 1991.